Perturbational estimation of geometry tolerances for rectangular integrated optics devices

M. Lohmeyer, N. Bahlmann, O. Zhuromskyy, P. Hertel

Department of Physics, University of Osnabrück,
Barbarastraße 7, D-49069 Osnabrück, Germany

ABSTRACT

Shifting the location of a dielectric boundary in the cross section of an integrated optical waveguide with piecewise constant refractive index profile results in a permittivity perturbation in a layer along the discontinuity line. On the basis of these thin layer perturbations, we discuss perturbational expressions for the derivatives of the propagation constants with respect to geometry parameters, both for fully vectorial, hybrid and for semivectorial approximations to the basic mode fields. The expressions are numerically verified by comparison with rigorously calculated data for a common semiconductor rib waveguide. Applied to a more complex device, the perturbational approach allows to estimate its complete set of tolerances for the geometry parameters, including the wavelength, on the basis of a single mode analysis. This is exemplified with a two rib waveguide coupler. By comparison with conventionally computed tolerances we give some assessment for the applicability of the effective perturbational approach.

Keywords: integrated optics, dielectric waveguides, guided modes, numerical modeling, fabrication tolerances

1. INTRODUCTION

Frequently, integrated optical devices rely on the interference of guided modes propagating along homogeneous waveguide sections. In first order perturbation theory, a slight alteration of a dimensional parameter influences the mode wavenumbers only while the mode amplitudes are almost unaffected. To estimate the deviation of the power transmission, it should be sufficient to consider only the propagation constant alteration, which amounts to calculating the mode wavenumber gradients with respect to geometry variables.

For a waveguide with piecewise constant permittivity profile, alteration of a dimensional parameter can be interpreted as a refractive index change in a thin layer along a dielectric discontinuity line. Based on such thin layer perturbations,[1] explicit expressions for the partial derivatives of the propagation constants with respect to dielectric boundary locations can be derived,[2] both for truly hybrid modes and for fields calculated in the semivectorial approximation. This is discussed in the first parts of the following section. In its remainder, we comment on the tight connection between the geometry parameters and the wavelength as the defining dimensional variable.

The perturbational expressions have been shown to be adequate for simple raised strip waveguides and raised strip couplers,[2] and in the framework of coupled mode theory.[3,4] These investigations were concerned with somehow exotic parameter sets for magnetic garnets, i.e. permittivity profiles of (3.6, 5.3, 1.0). In contrast, many integrated optics devices are realized with rib waveguides made of semiconductor material with typical refractive index profiles of e.g. (11.6, 11.8, 1.0), that is with a much lower permittivity contrast between substrate and the guiding film, but with a high contrast between the film and the surrounding air. At the relevant dielectric boundaries, either the field strength or the permittivity contrast is small, and it is not a priori obvious whether the perturbational expressions are numerically reliable in this case.

To answer this question, we choose a typical benchmark structure[5] for the numerical simulations in the first part of Section 3, where the perturbational wavenumber shifts are compared with numerically exact values. Likewise, the second part of Section 3 is concerned with working out the tolerance requirements for conventional two waveguide couplers based on these benchmark structures. We compare perturbational tolerances with conventionally, directly computed data.

Phone: +49/541/969-2641, Fax: +49/541/969-2670, E-mail: manfred.lohmeyer@physik.uni-osnabrueck.de

2. THEORY

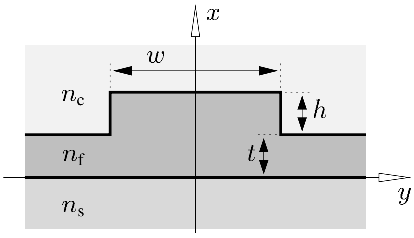

Figure 1. Typical rib waveguide. n_s, n_f, n_c, denote the refractive indices of the substrate, the film, and the cover layers. x and y are the transverse coordinate axes normal and parallel to the substrate surface, light propagates along the z direction.

Consider a simple rib waveguide as sketched in Figure 1, with piecewise constant permittivity profile $\epsilon = n^2$. Its hybrid guided mode fields

$$\boldsymbol{\mathcal{E}}(x, y, z, t) = \boldsymbol{E}(x, y) \exp(\mathrm{i}\omega t - \mathrm{i}\beta z), \quad \boldsymbol{\mathcal{H}}(x, y, z, t) = \boldsymbol{H}(x, y) \exp(\mathrm{i}\omega t - \mathrm{i}\beta z), \tag{1}$$

are given by the electric $\boldsymbol{E}$ and magnetic mode profile $\boldsymbol{H}$ and by the propagation constant β. They are governed by Maxwell's curl equations

$$(\mathrm{C} + \mathrm{i}\beta\mathrm{R})\boldsymbol{E} = -\mathrm{i}\omega\mu_0\boldsymbol{H}, \quad (\mathrm{C} + \mathrm{i}\beta\mathrm{R})\boldsymbol{H} = \mathrm{i}\omega\epsilon_0\epsilon\boldsymbol{E}, \tag{2}$$

where the curl operator has been split into a longitudinal part, βR and a part C acting on the transverse coordinates only,

$$\mathrm{C} = \begin{pmatrix} 0 & 0 & \partial_y \\ 0 & 0 & -\partial_x \\ -\partial_y & \partial_x & 0 \end{pmatrix}, \quad \mathrm{R} = \begin{pmatrix} 0 & 1 & 0 \\ -1 & 0 & 0 \\ 0 & 0 & 0 \end{pmatrix}. \tag{3}$$

μ_0 and ϵ_0 are the vacuum permeability and permittivity; the frequency ω is connected with the wavelength λ and wavenumber k by $\omega\sqrt{\epsilon_0\mu_0} = k = 2\pi/\lambda$.

Using these two operators and standard scalar product notation $(\boldsymbol{F}, \boldsymbol{G}) = \iint \boldsymbol{F}^*\boldsymbol{G}\,\mathrm{d}x\,\mathrm{d}y$, one can define[1] the following functional B_ϵ in terms of the six independent mode components $E_x, \ldots, H_z$:

$$\mathrm{B}_\epsilon(\boldsymbol{E}, \boldsymbol{H}) = \frac{\omega\epsilon_0(\boldsymbol{E}, \epsilon\boldsymbol{E}) + \omega\mu_0(\boldsymbol{H}, \boldsymbol{H}) + \mathrm{i}(\boldsymbol{E}, \mathrm{C}\boldsymbol{H}) - \mathrm{i}(\boldsymbol{H}, \mathrm{C}\boldsymbol{E})}{(\boldsymbol{E}, \mathrm{R}\boldsymbol{H}) - (\boldsymbol{H}, \mathrm{R}\boldsymbol{E})}. \tag{4}$$

B_ϵ is stationary if a valid mode field is inserted, i.e. for $\boldsymbol{E}$ and $\boldsymbol{H}$ satisfying Eqs. (2). In that case B evaluates to the propagation constant $\beta = \mathrm{B}_\epsilon(\boldsymbol{E}, \boldsymbol{H})$.

2.1. Thin Layer Perturbations

Now we take a closer look at a part of the waveguide cross section, as shown in Figure 2, with a horizontal dielectric boundary between y_0 and y_1, separating permittivities ϵ_- below and ϵ^+ above

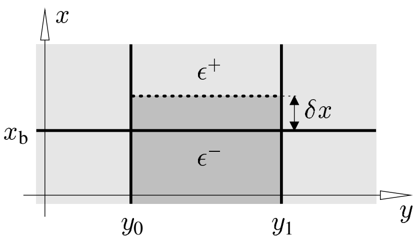

Figure 2. Shift of a horizontal boundary.

If the boundary is shifted from its original position x_b to the new position $x_b + \delta x$, the permittivity changes by

$$\delta\epsilon(x, y) = \begin{cases} \epsilon^- - \epsilon^+ & \text{for } (x, y) \in \square\,, \\ 0 & \text{otherwise}\,, \end{cases} \tag{5}$$

where the box symbol $\square$ indicates the rectangular region $x_b < x < x_b + \delta x$, $y_0 < y < y_1$.

Along with the permittivity, both the propagation constant and the mode fields change by small amounts $\delta\beta$, $\delta\boldsymbol{E}$, $\delta\boldsymbol{H}$, and the modified quantities are connected by the modified functional

$$\beta + \delta\beta = \mathrm{B}_{\epsilon+\delta\epsilon}(\boldsymbol{E} + \delta\boldsymbol{E}, \boldsymbol{H} + \delta\boldsymbol{H}). \tag{6}$$

$\mathrm{B}_{\epsilon+\delta\epsilon}$ is stationary at $\boldsymbol{E}+\delta\boldsymbol{E}, \boldsymbol{H}+\delta\boldsymbol{H}$. Therefore, if we suppose the original mode fields and the propagation constant to be known, for estimating the propagation constant shift it remains to supply plausible variations of the mode profiles.

Fortunately most of the components are continuous on the boundary, and one can simply choose the original fields as good estimates for the perturbed profiles: $\delta H_x = \delta H_y = \delta H_z = 0$, $\delta E_y = \delta E_z = 0$. However, the normal component of the dielectric displacement ϵE_x must be continuous, and E_x jumps in $x_{\rm b}$, from a level E_x^- to E_x^+. The new field has this jump transferred to $x_{\rm b}+\delta x$, thus E_x must be modified by

$$\delta E_x(x,y) = \begin{cases} \dfrac{\epsilon^+ - \epsilon^-}{\epsilon^-} & \text{for } (x,y) \in \Box\,, \\ 0 & \text{otherwise}\,. \end{cases} \tag{7}$$

This is illustrated in Figure 3.

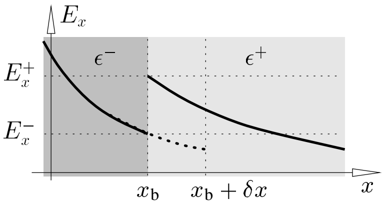

Figure 3. Boundary shift from $x_{\rm b}$ to $x_{\rm b}+\delta x$. E_x changes from the continuous to the dotted curve.

With these quantities substituted into functional (6), and terms $\sim \delta\beta\delta\boldsymbol{E}$ neglected, one arrives at an expression for the shift of the propagation constant due to a thin layer perturbation[1]:

$$\delta\beta = \frac{\omega\epsilon_0}{2} \frac{(\epsilon^- - \epsilon^+) \displaystyle\iint_\Box \left(\frac{\epsilon^+}{\epsilon^-}|E_x|^2 + |E_y|^2 + |E_z|^2\right)\,\mathrm{d}x\,\mathrm{d}y}{\displaystyle\iint \left(E_x H_y^* - E_y H_x^*\right)\,\mathrm{d}x\,\mathrm{d}y}\,. \tag{8}$$

2.2. Geometry Perturbation Formulas

For small δx the surface integration over the box region can be replaced by a line integral along the dielectric boundary. Now the equation gives directly the derivative of the propagation constant with respect to the boundary location

$$\delta\beta = \frac{\omega\epsilon_0}{2} \frac{(\epsilon^- - \epsilon^+) \displaystyle\int_{y_0}^{y_1} \left((E_x^+)^* E_x^- + |E_y|^2 + |E_z|^2\right)(x_{\rm b}, y)\,\mathrm{d}y}{\displaystyle\iint \left(E_x H_y^* - E_y H_x^*\right)\,\mathrm{d}x\,\mathrm{d}y}\,\delta x\,. \tag{9}$$

This is at least a plausible expression. The propagation constant is influenced only if there is a discontinuity in the permittivity, and if the mode field does not vanish on the boundary. Only well defined quantities enter, there are no ambiguities regarding the discontinuity of E_x (note, that the first term in the denominator is alternatively $(E_x^+)^* E_x^- = \epsilon^+|E_x^+|^2/\epsilon^- = \epsilon^-|E_x^-|^2/\epsilon^+ = |\epsilon E_x|^2/(\epsilon^-\epsilon^+)$). Fortunately the result remains the same, if one starts with a downwards moved boundary and rewrites Eqs. (5) and (7) accordingly.

Frequently calculations are performed in semivectorial approximation.[6] A semivectorial TE-polarized field is given by its dominant E_y component, with E_x assumed to vanish. For our piecewise constant profiles, it is defined as a field E_y satisfying the wave equation $(\partial_x^2 + \partial_y^2 + k^2\epsilon - \beta^2)E_y = 0$ inside the homogeneous rectangles, with continuous fields E_y, $\partial_x E_y$ on horizontal boundaries and ϵE_y, $\partial_y E_y$ on vertical boundaries. Inserted into Eq. (9), this ansatz yields

$$\delta\beta = \frac{k_0^2}{2\beta} \frac{(\epsilon^- - \epsilon^+) \displaystyle\int_{y_0}^{y_1} \left(|E_y|^2 + \beta^{-2}|\partial_y E_y|^2\right)(x_{\rm b}, y)\,\mathrm{d}y}{\displaystyle\iint \left(|E_y|^2 - \beta^{-2} E_y \partial_y^2 E_y^*\right)\,\mathrm{d}x\,\mathrm{d}y}\,\delta x\,. \tag{10}$$

If one neglects the derivative $\beta^{-1}\partial_y E_y$ on the relevant horizontal boundary, Eq. (10) simplifies to

$$\delta\beta = \frac{k_0^2}{2\beta} \frac{(\epsilon^- - \epsilon^+) \displaystyle\int_{y_0}^{y_1} |E_y|^2(x_\mathrm{b}, y)\,\mathrm{d}y}{\displaystyle\iint |E_y|^2 \mathrm{d}x\,\mathrm{d}y}\,\delta x\,. \tag{11}$$

For TM-polarization, ususally all components are expressed by the dominant magnetic component H_y, with H_x set to zero. The dominant magnetic component H_y satisfies the wave equation everywhere except on the boundaries, where H_y and $\epsilon^{-1}\partial_x H_y$ are continuous for a horizontal line, and with continuous H_y and $\partial_y H_y$ on vertical lines. Now Eq. (9) yields

$$\delta\beta = \frac{\beta}{2} \frac{(\epsilon^- - \epsilon^+) \displaystyle\int_{y_0}^{y_1} \left(\frac{1}{\epsilon^-\epsilon^+}|H_y - \beta^{-2}\partial_y^2 H_y|^2 + \beta^{-4}|\partial_y \frac{1}{\epsilon}\partial_x H_y|^2 + \beta^{-2}|\frac{1}{\epsilon}\partial_x H_y|^2\right)(x_\mathrm{b}, y)\,\mathrm{d}y}{\displaystyle\iint \frac{1}{\epsilon}\left(H_y - \beta^{-2}\partial_y^2 H_y\right) H_y^*\,\mathrm{d}x\,\mathrm{d}y}\,\delta x \tag{12}$$

for the propagation constant shift of a quasi TM mode due to a horizontal boundary displacement. Again all quantities in the denominator are well defined, since the inverse permittivity times the normal derivative of H_y is continuous on the horizontal boundary.

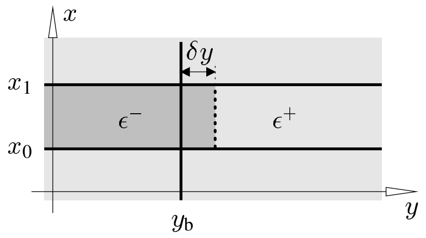

Figure 4. Shift of a vertical boundary.

Analogous equations hold for shifting vertical boundaries. Figure 4 illustrates the relevant geometry. Moving the boundary between permittivities ϵ^- on the left and ϵ^+ on the right form y_b to $y_\mathrm{b} + \delta y$ changes the propagation constant of a hybrid, arbitrarily polarized mode by

$$\delta\beta = \frac{\omega\epsilon_0}{2} \frac{(\epsilon^- - \epsilon^+) \displaystyle\int_{x_0}^{x_1} \left(|E_x|^2 + (E_y^+)^* E_y^- + |E_z|^2\right)(x, y_\mathrm{b})\,\mathrm{d}x}{\displaystyle\iint \left(E_x H_y^* - E_y H_x^*\right)\,\mathrm{d}x\,\mathrm{d}y}\,\delta y\,. \tag{13}$$

For semivectorial TE-polarized fields, it is usually no longer possible to skip the y-derivative, since the maxima of the longitudinal electric component $E_z = -\mathrm{i}\beta^{-1}\partial_y E_y$ are located on the rib flanks. The expression for the wavenumber shift of a quasi TE mode reads

$$\delta\beta = \frac{k_0^2}{2\beta} \frac{(\epsilon^- - \epsilon^+) \displaystyle\int_{x_0}^{x_1} \left((E_y^+)^* E_y^- + \beta^{-2}|\partial_y E_y|^2\right)(x, y_\mathrm{b})\,\mathrm{d}x}{\displaystyle\iint \left(|E_y|^2 - \beta^{-2} E_y \partial_y^2 E_y^*\right)\,\mathrm{d}x\,\mathrm{d}y}\,\delta y \tag{14}$$

For semivectorial TM modes there is a problem. While the fields satisfy the continuity requirements for H_y and H_z exactly, the continuity requirements for E_x and E_z on vertical boundaries are significantly violated. Thus Eq. (13) can not be expected to give good results with a quasi TM field inserted. However, the TM-problem, if restricted to vertical boundaries, should be equivalent to the TE-problem with horizontal boundaries. Therefore a plausible expression for the TM wavenumber shift due to the displacement of a vertical boundary is Eq. (10), with E_y substituted by H_y:

$$\delta\beta = \frac{k_0^2}{2\beta} \frac{(\epsilon^- - \epsilon^+) \displaystyle\int_{x_0}^{x_1} |H_y|^2(x, y_\mathrm{b})\,\mathrm{d}x}{\displaystyle\iint |H_y|^2 \mathrm{d}x\,\mathrm{d}y}\,\delta y\,. \tag{15}$$

At least for the structures considered in this and the previous paper,[2] we have found Eq. (15) to be correct up to the same accuracy as the expressions for TE and hybrid modes.

The standard rib waveguide as sketched in Figure 1 is defined by three geometry variables: the rib width w, its height h and the thickness t of the remaining film besides the rib. We are interested in the partial derivatives $\partial_h\beta$, $\partial_t\beta$, and $\partial_w\beta$. The two former are obtained by applying one of Eqs. (9, 10, 11, 12) to the top of the rib or to the rib baseline, respectively. Using Eqs. (13, 14, 15) with one of the rib flanks yields $\partial_w\beta$. This approach extends in an obvious way to the coupler structures discussed in the last section and to other, more complex geometries. Usually, the perturbational formulas must be applied to more than one boundary section to compute the derivatives with respect to a general model variable.

2.3. Wavelength

For the rib waveguide of Figure 1, the relevant dimensional parameters are w, h, t, and the wavelength λ. The propagation constant is a homogeneous function of degree -1 in these parameters, i.e. for an arbitrary factor a the equality $\beta(a\lambda, ah, aw, at) = \beta(\lambda, h, w, t)/a$ holds. Thus the partial derivatives are connected by

$$\partial_\lambda\beta = -\frac{1}{\lambda}\left(\beta + h\partial_h\beta + w\partial_w\beta + t\partial_t\beta\right). \tag{16}$$

Therefore, the perturbational expressions Eqs. (9–15) give direct access to the derivative with respect to the wavelength as well. Note, that Eq. (16) assumes all material parameters to be fixed. A pronounced wavelength dependence e.g. of one of the refractive indices must be taken into account by a combination of perturbation formulas or by explicit numerical evaluation.

3. NUMERICAL RESULTS

In this investigation, we have employed a recently proposed mode solver[7] for computing the unperturbed mode fields and propagation constants and for generating the reference data. The method is based on local plane wave expansions for regions with constant permittivity. It yields quasianalytical representations of the mode fields which take field discontinuities on dielectric interfaces explicitely into account and allow for a convenient evaluation of the various line and surface integrals.

3.1. Rib Waveguides

Numerical assessment for the perturbational expressions of the former section starts with the modes for the unperturbed waveguide. Figure 5 shows intensity profiles for the fundamental modes of both polarizations for a benchmark rib waveguide.[5] The corresponding propagation constants are $\beta_*^{\mathrm{TE}} = 18.6481\,\mu\mathrm{m}^{-1}$ for TE polarization and $\beta_*^{\mathrm{TM}} = 18.6475\,\mu\mathrm{m}^{-1}$ for the TM mode, computed in the semivectorial approximation.

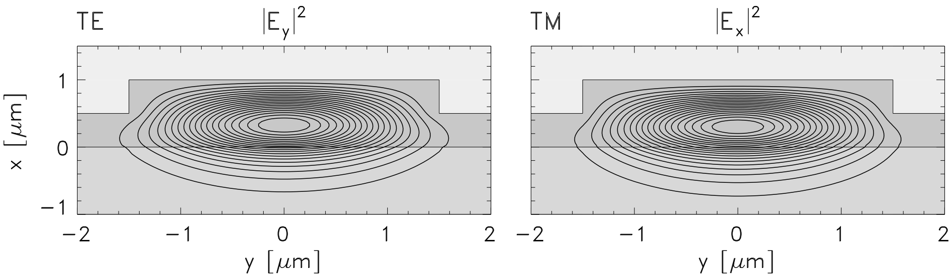

Figure 5. Intensity profiles for the dominant components of the semivectorial TE (left) and TM (right) polarized modes for a rib waveguide according to Figure 1. Contour levels are spaced by 5% of the maximum intensity. Parameters are: $h = 0.5\,\mu$m, $w = 3.0\,\mu$m, $t = 0.5\,\mu$m, $\lambda = 1.15\,\mu$m, $n_{\mathrm{s}} = 3.40$, $n_{\mathrm{f}} = 3.44$, and $n_{\mathrm{c}} = 1.0$.

Beginning with the parameter set as given for Figure 5, we have varied separately one of the parameters h, w, t, or λ, and recalculated the propagation constants, keeping all other parameters fixed. Alternatively, applying the perturbational expressions from Section 2 to the mode profiles of Figure 5 or to the corresponding fully vectorial fields should yield propagation constant gradients $\partial_q\beta$, evaluated for the original structure $\delta q = 0$ for parameters $q \in \{h, w, t, \lambda\}$. Figures 6 and 7 compare the corresponding linear approximations $\beta(\delta q) = \beta(0) + \delta q\partial_q\beta$ with the directly computed data.

Obviously the perturbational secants are almost tangents to the reference curves, the marker lines, as it was intended. The good agreement, both for fully vectorial basic fields and for the semivectorial fields, can be viewed as a confirmation for the

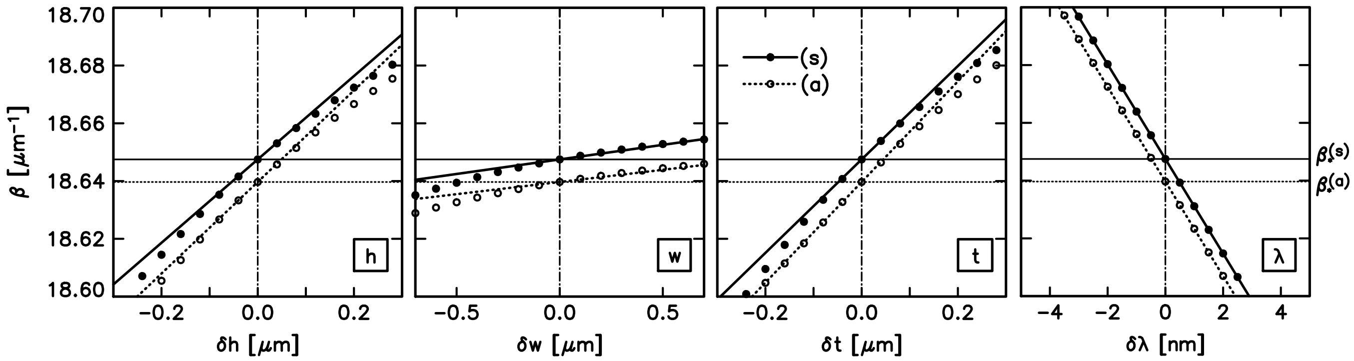

Figure 6. Dependence of the propagation constants on variations of the rib height δh, of the rib width δw, of the film thickness besides the rib δt, and of the wavelength $\delta\lambda$, for the fundamental hybrid symmetric ((s), continuous lines, filled circles; fields H_x, E_y, H_z are even with respect to $y \to -y$, other components are odd) and antisymmetric ((a), dotted lines, open circles, opposite symmetry of all fields) mode of a rib waveguide with parameters as given for Figure 5. Marker points indicate values computed directly for the modified structures, lines show the tangents predicted by the perturbational theory.

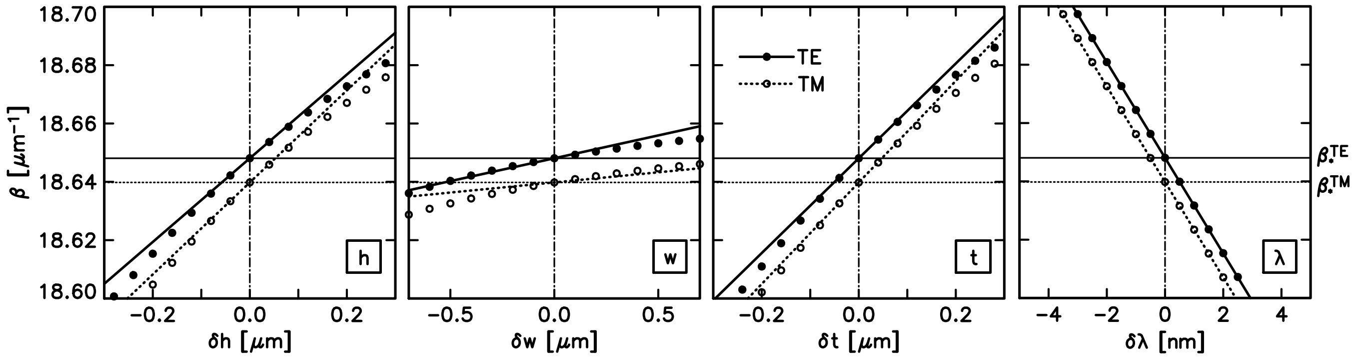

Figure 7. Analogon to Figure 6 for the fundamental TE and TM modes computed with the semivectorial approximation. Symbols and parameters are as given in the caption of Figures 6 and 5.

perturbation formulas. The small remaining deviations should be partly due to the approximations entering the derivation in Section 2, and partly due to the inaccuracies in the numerically computed basic modes.

Therefore, at the same time this comparison can be regarded a good check for the mode solver if one accepts Eqs. (9–15) to be correct. The test combines propagation constants and mode profiles at critical points, the dielectric interfaces. It is a self consistent test requiring no reference data.

Frequently there is more than one way to apply the perturbational expressions. For example, w can be varied by shifting alternatively the right or the left rib sidewall (inverting the result). Since all modes have a definite symmetry, the results are exactly equal. The same can be done for the strip height: lifting the top rib boundary should be equivalent to lowering the rib baseline. And now it is no longer obvious that the results agree. We have tested this for rib waveguide of Figure 5, and found no visible change with respect to Figures 6 and 7.

Among the four parameters, the wavelength has the most pronounced influence on the propagation constants. In contrast to the formerly investigated structures,[2–4] the wavelength dependence of the propagation constant is given by the inverse wavelength itself. $\partial_\lambda \beta = -\beta/\lambda$ is a good approximation for the present waveguide. Due to either the small field strength on the rib flanks and on the surface (w, h) or to the low refractive index contrast between substrate and film (h, t), the other contributions to Eq. (16) remain small ($\approx 0.2\,\mu\mathrm{m}^{-1}$) when compared with the propagation constant ($\approx 18.6\,\mu\mathrm{m}^{-1}$).

3.2. Rib Waveguide Coupler

As sketched in Figure 1, the central part of a directional coupler made of two of the former rib waveguides is characterized by one additional parameter, the separation g of the ribs.

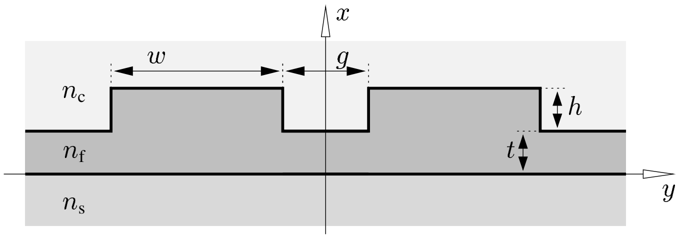

Figure 8. Cross section of the two rib waveguide coupler. The structure is meant to be symmetric with respect to $y \rightarrow -y$.

For each polarization, the structure supports one mode of even and one of odd symmetry. Figure 9 illustrates the corresponding TE mode profiles; similar plots for TM fields are almost indistinguishable.

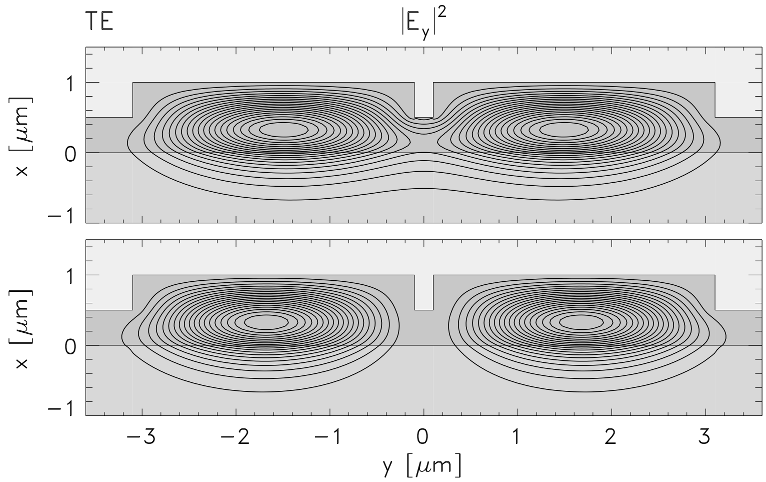

Figure 9. Intensity profiles for the semivectorial TE modes of even (top) and odd symmetry (bottom) in a two rib coupler according to Figure 8. Parameters are as given for Figure 5, with a gap spacing $g = 0.2\,\mu$m.

For fixed polarization, let ϕ_l and ϕ_r denote the mode of the left respectively right isolated waveguide. ψ_s and ψ_a are the symmetric and antisymmetric supermode of the entire structure. We suppose the coupling region to be excited by the single mode ϕ_l of the left waveguide, normalized to an input power of one. Neglecting reflection and radiation at input and output, the relative power

$$P(L) = w_\mathrm{s}^2 + w_\mathrm{a}^2 + 2w_\mathrm{s}w_\mathrm{a}\cos((\beta_\mathrm{s} - \beta_\mathrm{a})L) \tag{17}$$

is transferred to the opposite waveguide mode ϕ_r after propagation along the device length L. The weight factors are given by mode overlaps $w_j = \langle \phi_\mathrm{r}, \psi_j \rangle \langle \psi_j, \phi_\mathrm{l} \rangle$, $j = \mathrm{s, a}$ at input and output, where $\langle\, .\, ,\, .\, \rangle$ is a bilinear product suitable to express supermode orthogonality. All modes are meant to be normalized with respect to this product. Without loss of generality, the weights are real with different signs.

If the device length is set to $L_\mathrm{c} = \pi/(\beta_\mathrm{s} - \beta_\mathrm{a})$, the transferred power is maximum and close to unity, provided that all parameters are kept at their original values. If one of them is slightly detuned, a smaller amount of power will be coupled to the right channel. This dependence is shown in Figure 10. For otherwise fixed geometry, we have varied one dimensional parameter and repeated the entire calculation, including mode field composition and overlap integration. The results are indicated by the marker points.

The lines in Figure 10 show the results of the perturbational theory. For tuned parameters, we have calculated the wavenumber gradients $\partial_q \beta_\mathrm{s}$, $\partial_q \beta_\mathrm{a}$, $q \in \{h, w, t, g, \lambda\}$ using Eqs. (10, 12, 14, 15). Then approximations for the transferred power Eq. (17) were assembled with the unperturbed weights, but with altered propagation constants $\beta_\mathrm{s,a} + \delta q \partial_q \beta_\mathrm{s,a}$.

At least for the rib height and the outer film thickness, perturbational and reference results agree well. Evaluating the perturbational wavenumber gradients includes integration along lines with comparably large field strength, where the relative error in the basic mode field can be assumed to be small. On the other hand, for rib width, gap spacing, and, consequently, wavelength, the field must be integrated along the rib sidewalls, where the modal field is almost vanishing. Nevertheless the

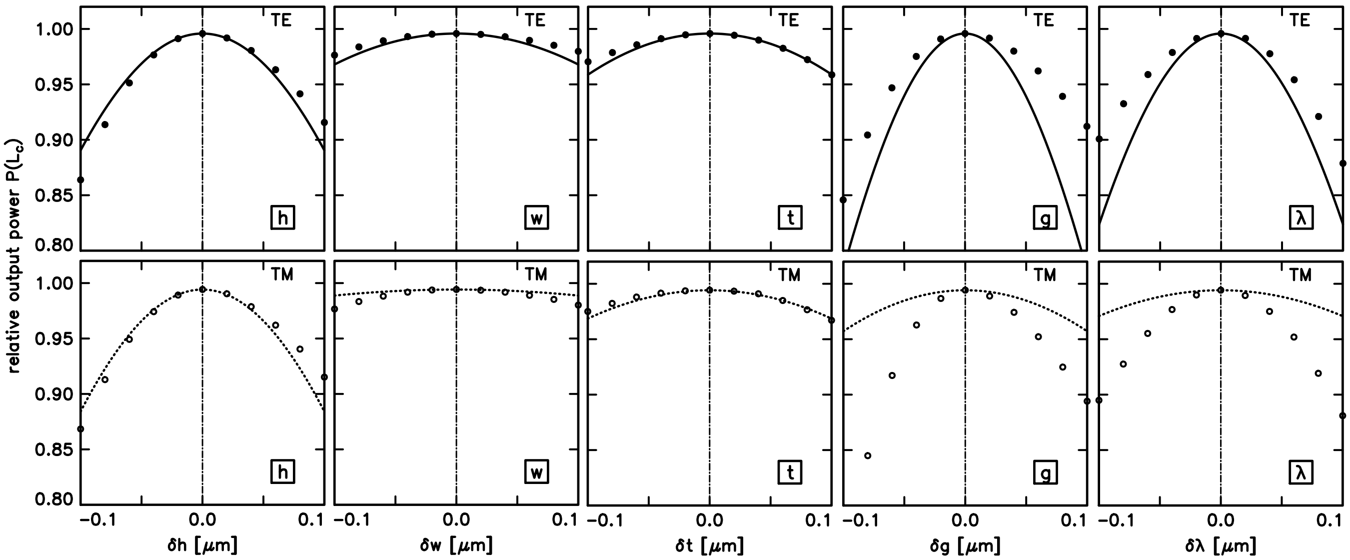

Figure 10. Influence of parameter variations on the relative output power $P(L_\mathrm{c})$ of a rib waveguide coupler as sketched in Figure 8, for TE (top row) and TM polarization (bottom row). One of $q \in \{h, w, t, g, \lambda\}$ is altered to $q + \delta q$, with the remaining parameters as given for Figure 9. Markers correspond to complete semivectorial analysis runs; the lines are perturbational results. $L_\mathrm{c} = 650\,\mu$m for TE and $L_\mathrm{c} = 599\,\mu$m for TM polarization.

same absolute error in the basic field must be assumed, resulting in a higher relative error level of the small wavenumber gradients with respect to these variables.

Another source of error may be expected in the semivectorial approximation. While the continuity conditions on horizontal boundaries are obeyed exactly, the fields violate the conditions on the vertical boundaries, which are directly relevant for the gradients with respect to w and g (cf. the remarks in Section 2).

		TE	TM	TE	TM	TE	TM	TE	TM	TE	TM
		$\partial_h\beta/\mu\mathrm{m}^{-2}$		$\partial_w\beta/\mu\mathrm{m}^{-2}$		$\partial_t\beta/\mu\mathrm{m}^{-2}$		$\partial_g\beta/\mu\mathrm{m}^{-2}$		$\partial_\lambda\beta/\mu\mathrm{m}^{-2}$	
(s)	FD	0.137	0.151	0.010	0.009	0.168	0.179	−0.006	−0.008	−16.382	−16.383
	PT	0.138	0.151	0.013	0.006	0.167	0.179	−0.009	−0.004	−16.398	−16.384
(a)	FD	0.147	0.162	0.015	0.013	0.162	0.174	0.004	0.004	−16.392	−16.394
	PT	0.148	0.163	0.018	0.008	0.161	0.173	0.005	0.002	−16.411	−16.389
$\Delta P = 1\%$		$\Delta h/$nm		$\Delta w/$nm		$\Delta t/$nm		$\Delta g/$nm		$\Delta\lambda/$nm	
$L = L_\mathrm{c}$	NUM	29	28	74	77	52	61	28	23	30	28
	PT	30	29	59	135	51	62	21	51	23	64

Table 1. For the coupler of Figures 8 to 10:
Top: partial derivatives of the supermode propagation constants, for the mode with even (s) and odd symmetry (a), and for TE and TM polarization. Values 'FD' are calculated as difference quotients from mode analysis runs on neighbored parameter sets. 'PT' are the results form using Eqs. (10, 12, 14, 15) with the unperturbed modes.
Bottom: Geometry tolerances admissible for a power transfer deviation ΔP of less than 1%. 'NUM' gives directly computed limits, 'PT' are values estimated with Eq. (18) and the perturbational formulas of Section 2.

However, as indicated by the top part of Table 1, the propagation constant derivatives are evaluated correctly up to $0.005\,\mu\mathrm{m}^{-2}$ for all dimensional variables and for both TE and TM polarization. Unfortunately, the relevant quantity for tolerance investigations is the difference between the wavenumber gradients of the even and odd supermode. This becomes evident if Eq. (17) is expanded with respect to δq. Assuming fixed weigths $|w_\mathrm{s}| = |w_\mathrm{a}| = 1/2$, there is an interval $-\Delta q < \delta q < \Delta q$ for the allowed parameter detuning such that the power transmission deviates by no more than ΔP from the value for reference parameters:

$$\Delta q = \frac{2\sqrt{\Delta P}}{L\,|\partial_q \beta_{\rm s} - \partial_q \beta_{\rm a}|}. \tag{18}$$

The bottom part of Table 1 compares these perturbational tolerances with values read from the (interpolated) marker curves of Figure 10. Obviously, the perturbational wavenumber gradients give good estimates for the rib height and film thickness tolerances. For the rib width, gap spacing, and wavelength tolerances, at least the order of magnitude is correct.

4. CONCLUSIONS

Propagation constant gradients with respect to alterations of geometry variables can be estimated by line integrals of the mode profiles along the relevant dielectric interfaces. This requires one single mode analysis only, independent of the number of geometry parameters in the actual structure. The expressions provide direct access to the wavelength dependence.

For a common rib waveguide, the perturbationally evaluated gradients agree well with conventional finite difference approximations. This test, together with comparison of gradients from equivalent boundary movements, is a sensitive self consistency check for the underlying mode solver.

The perturbational expressions allow tolerance estimations for realistic integrated optical devices at almost no extra computational cost. This was demonstrated by the example of a two rib waveguide directional coupler. It must be emphasized, that accurate basic mode fields are required. Regarding automated device optimization, the expressions give access at least to estimates for the partial derivatives of the objective function, the transmitted power. In cases where a single mode computation is expensive, this may significantly reduce the computational effort.

ACKNOWLEDGMENTS

Financial support by Deutsche Forschungsgemeinschaft (Sonderforschungsbereich 225) is gratefully acknowledged.

REFERENCES

1. C. Vassallo, *Optical Waveguide Concepts*, Elsevier, Amsterdam, 1991.
2. M. Lohmeyer, N. Bahlmann, and P. Hertel, “Geometry tolerance estimation for rectangular dielectric waveguide devices by means of perturbation theory,” *Optical and Quantum Electronics* , 1998. Submitted.
3. M. Lohmeyer, N. Bahlmann, O. Zhuromskyy, and P. Hertel, “Phase-matched rectangular magnetooptic waveguides for applications in integrated optics isolators: numerical assessment,” *Optics Communications*, 1998. Accepted for publication.
4. M. Lohmeyer, N. Bahlmann, O. Zhuromskyy, and P. Hertel, “Radiatively coupled waveguide polarization splitter simulated by wave-matching based coupled mode theory,” *Optical and Quantum Electronics* , 1998. Submitted.
5. C. Vassallo, “1993-1995 Optical mode solvers,” *Optical and Quantum Electronics* **29**, pp. 95–114, 1997.
6. M. S. Stern, “Semivectorial polarised finite difference method for optical waveguides with arbitrary index profiles,” *IEE Proceedings, Pt. J* **135**(1), pp. 56–63, 1988.
7. M. Lohmeyer, N. Bahlmann, O. Zhuromskyy, and P. Hertel, “Wave-matching-simulations of integrated optical coupler structures” and references cited therein, this volume.